Fuel savings for a general cargo ship employing retractable bow foils

Eirik Bøckmann, Audun Yrke and Sverre Steen

February 18, 2018

Abstract

Route simulations were performed on a 100 m long (between perpendiculars) general cargo ship equipped with retractable bow-mounted foils, so-called wavefoils, for resistance reduction and motion damping in waves. Two round-trip routes were simulated: Orkney Islands to Iceland and across the Bay of Biscay. Ship motions and added resistance in waves were calculated in the frequency domain. Foil thrust was calculated in the time domain, based on a frequency-domain model of the vessel motions with wavefoils, using a slightly modified version of the Leishman-Beddoes dynamic stall model (Leishman and Beddoes, 1989). For both directions of each route, 1000 journeys with and without wavefoils were simulated, with wind and wave conditions obtained from ECMWF hindcast data. In the simulations, two identical ships, one equipped with wavefoils and the other without, were assumed operating in parallel, starting their journeys at random times between January 1, 2000, and December 1, 2014. The brake power was constant for the ship without wavefoils, whereas the ship with wavefoils reduced its power to obtain the same speed as the ship without wavefoils. For the most favorable route with respect to this study, Orkney Islands to Iceland, the average fuel saving was 22% for a constant brake power without foils that corresponds to a calm-water speed of 14 knots.

1 Introduction

The environmental motivations for reducing a ship's fuel consumption are obvious and well known and do not require further elaboration. Lower fuel consumption also implies lower operating costs for the ship owner. One promising way of saving fuel for ships operating in areas with strong seaways is employing bow foils for resistance and motion reduction in waves. Such foils, known as wavefoils, work best for wavelength-to-shiplength ratios bewteen between 1 and 2 (Naito and Isshiki, 2005; Bøckmann, 2015). Typical spectral peak periods (T_p) in the North Atlantic from 7–15 s imply wavelengths of 76–351 m based on T_p, or 45–208 m based on the mean period (T_{m01}). Therefore, the optimal ship length for a ship employing wavefoils in this region can be said to be in the 50–150 m range. The present paper presents simulated energy savings, or fuel savings, for a general cargo vessel in this length range employing wavefoils on two round-trip routes.

Published studies on achievable mean fuel savings for ships employing wavefoils in realistic ocean wave conditions are very limited. Veritec, a former subsidiary of Det Norske Veritas (today DNV GL Group) analyzed the propulsive effect of wavefoils on vessels of lengths 20 m, 40 m, and 70 m (Veritec, 1985, 1986), operating in the North Sea. Total foil areas of 2%, 4% and 6% of the vessel water plane area were studied. The fuel saving percentage increased with increasing foil area for all three ships. For the 70 m vessel with a foil of 6% of the vessel water plane area, the fuel saving was 43% at 10.6 knots and 10% at 15.9 knots. The vessel motions were calculated using a strip theory program, but the heave and pitch damping due to the foils was not accounted for. Furthermore, neither drag nor dynamic lift effects were accounted for.

Naito and Isshiki (2005) presented a graph of speed loss as a function of significant wave height (H_S) for a ship with and without wavefoils, but only for one mean wave period. They also state that "Economical advantage of bow wings has not been demonstrated". Angvik (2009) and Borgen (2010) calculated fuel savings for an offshore supply vessel employing wavefoils. Borgen also studied a coastal tanker and a purse seiner. They obtained the ship motions with and without foils from the frequency-domain module VERES of the computer program ShipX from SINTEF Ocean (formerly MARINTEK). Foil drag and finite span effects were accounted for, but stall was neglected since the foils were assumed to be actively controlled in pitch. Borgen used a simple correction for unsteady effects and he also assumed a benefit of chordwise flexibility. Of the two, only Borgen studied irregular waves, with wave directions from head to following sea in steps of 45 degrees, but he only considered one significant wave height (2.51 s) and one mean zero-up-crossing period (6.77 s). The reported fuel savings were large and so were the foils considered: For instance, for the offshore supply vessel, Borgen found that the fuel saving averaged over all wave directions was 39% at 10 knots and 24% at 15 knots, when employing foils with a total foil planform area of 6% of the vessel's water plane area and a span-to-chord-ratio (span being the distance from foil root to tip) of 5.

Bøckmann (2015) calculated fuel savings for a platform supply vessel equipped with a large wavefoil underneath the bow in his PhD thesis. A two-way coupling between non-harmonically varying foil forces and the ship motions, meaning that the foil forces affect the ship motions and vice versa, was obtained by implementing a dynamic stall model for the foil forces in the time-domain ship seakeeping and maneuvering simulator VeSim from SINTEF Ocean. Fuel savings were calculated in short-crested irregular waves for wave directions ranging from head to following sea in steps of 45 degrees, but only for one significant wave height (H_S) and three values of T_p. The fuel saving was 9% when averaged over all wave directions, for a ship speed of 12 knots and a significant wave height of 2.5 m. To calculate the speed loss or power saving for a motorized vessel employing wavefoils on a given route, the speed-power curve must be obtained for all combinations of sea state and wave direction, which makes such an analysis extremely time consuming, unless the approach in the present work is adopted.

With this background in mind, the motivation for the present paper was to answer the question "What is the fuel saving with wavefoils?" by calculating mean fuel savings for selected routes – not only selected wave conditions – for a ship with realistically large wavefoils. In the present work, we also compare three different models for calculating the foil thrust. We show that calculating the ship motions in the frequency domain and the foil forces in the time domain,

with a one-way coupling from ship motions to foil thrust, give conservative fuel saving results relative to simulating two-way-coupled ship motions and foil thrust in the time domain. The latter approach was compared with experiment results in Bøckmann (2015) and Bøckmann and Steen (2016).

2 Case vessel

The vessel studied in the present work, illustrated in Fig. 1 with the wavefoils deployed, is a general cargo vessel designed by the second author. Main particulars of the vessel are given in Table 1.

Length overall	110.39 m
Length betw. perp.	99.90 m
Length on waterline	106.61 m
Breath on waterline	19.39 m
Draught at amidships	6.00 m
Volume displacement	7,706.41 m^3
Wetted surface area	2,588.62 m^2
Water plane area	1,687.55 m^2
Projected front area above the waterline	400 m^2
Projected side area above the waterline	1161 m^2
Water plane area coefficient	0.816
Prismatic coefficient	0.616
Block coefficient	0.612
Midship coefficient	0.993
Main engine power (MCR)	3900 kW
Service speed	14 knots

Table 1: Main particulars of the case vessel.

The wavefoils – or simply referred to as "the foils" – with main particulars given in Table 2, are mounted to the ship with the span axis sloping 6 degrees tip-down and a fixed pitch angle of 0 degrees when deployed. The foils have no sweep angle relative to the quarter-chord, and the horizontal distance from the aft perpendicular to the quarter-chord of the foils is 94.448 m. The total foil planform area is 2.6% of the ship's water plane area.

The foils can be retracted through apertures in the hull. The additional resistance that these apertures are causing is neglected in the present work.

Profile	NACA 0015
Length	8.50 m
Inner chord	3.20 m
Outer chord	2.00 m
Foil area	22.10 m^2
Planform	Tapered

Table 2: Main particulars of the wavefoils

Figure 1: The case vessel with wavefoils deployed

3 Routes

Two different routes were studied, see Fig. 2. These routes were chosen because they are frequently sailed by ships in the same size range as the case vessels and because they are particularly wave-rich. The two routes both follow great circle routes and their start and end coordinates are given in Table 3.

Route	**Start coordinates**	**End coordinates**
A	59.4841°N, -2.4390°E	63.7457°N, -22.8531°E
B	43.1384°N, -9.5786°E	49.1788°N, -5.1311°E

Table 3: Start and end coordinates of the routes

Route A goes from north of the Orkney Islands to near Reykjavik, and route B goes across the Bay of Biscay. Route B has very high ship traffic density since it is part of the standard sailing route between Southern and Northern Europe. The reason why the routes are great-circle segments instead of port-to-port routes is that the authors wanted each route to be representative of the wave conditions in one distinct sea area.

4 Simulation model

4.1 Overview of the model

The frequency-domain module VERES (Fathi, 2014) of the computer program ShipX from SINTEF Ocean was used to calculate the ship's response amplitude

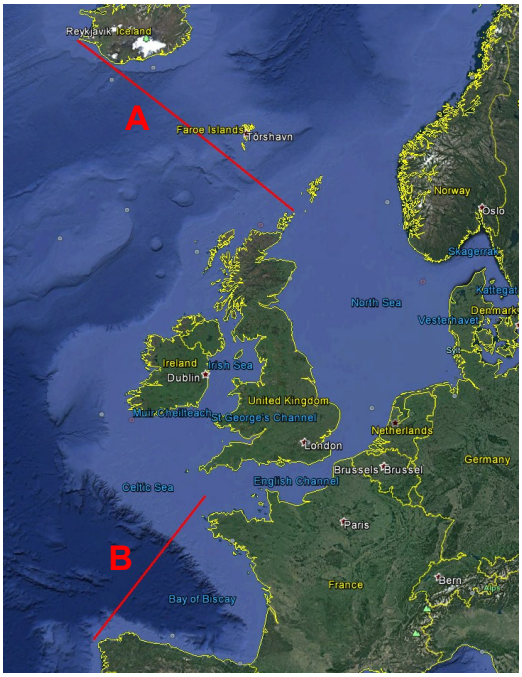

Figure 2: Routes studied

operators (RAOs) and the added resistance due to waves, with and without wavefoils. VERES is based on linear potential strip theory (Salvesen et al., 1970). VERES includes a frequency-domain model for the foil forces (Fathi, 2014), accounting for dynamic effects on the foil lift through the Theodorsen function (Theodorsen, 1935). Due to the limitations of frequency-domain simulations (see Bøckmann and Steen (2016)), however, this foil model implies that the foil force component parallel to the chord, i.e., the chordwise force (see Fig. 3), as well as stall are neglected. Therefore, the chordwise force must be calculated separately.

The wavefoils were assumed to be fixed, i.e., having no active or passive regulation of the pitch. Fixed foils are subject to stall if the angle of attack is large enough. To account for this, the foil thrust was calculated by using the same dynamic stall model as described in Bøckmann (2015), with the modifications described in Bøckmann and Steen (2016). Note that since foil stall is not modeled in VERES, foil stall was not accounted for when calculating the motions of the ship with foils, which was used as input to the dynamic stall model for the foil thrust. The consequence of this is that the predicted ship motions with foils will be smaller than in reality, since the foils provide larger damping when stall does not occur.

The brake power in a given sea condition, P_{Bw}, was calculated as

$$P_{Bw} = \frac{(R_{Tw} - T_{foils})\, V}{\eta_{Dw}\eta_S}, \tag{1}$$

where R_{Tw} is the ship resistance in the given sea condition (accounting for the

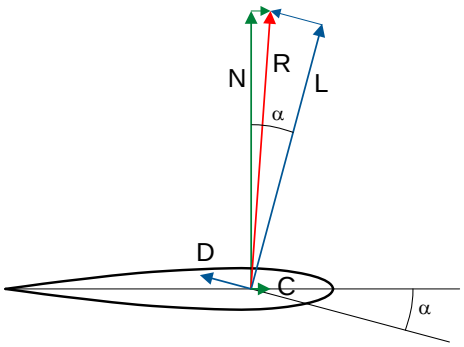

Figure 3: The relation between lift (L), drag (D), normal (N) and chordwise (C) force and the resultant force (R) (Bøckmann and Steen, 2013). α is the angle of attack.

motion-damping effect of the foils but not the foil thrust), T_{foils} is the foil thrust, V is the ship speed, η_{Dw} is the propulsion efficiency in waves, and η_S is the transmission efficiency. R_{Tw} is given as

$$R_{Tw} = R_T + \Delta R_{wind} + \Delta R_{wave}, \tag{2}$$

where R_T is the calm-water resistance without foils, ΔR_{wind} is the added resistance due to wind and ΔR_{wave} is the added resistance due to waves. R_T was obtained using the empirical resistance prediction method of Hollenbach (1998).

In the present work, $\eta_S = 0.97$ and $\eta_{Dw} = 0.6$ were used, as these are typical values of transmission efficiency and propulsion efficiency (Lützen and Holmegaard, 2012; Faltinsen, 2005). The calm-water brake power without foils, P_B, was calculated from Eq. 1, with $R_{Tw} = R_T$, $T_{foils} = 0$ and $\eta_{Dw} = \eta_D$, where η_D is the propulsion efficiency in calm water. η_{Dw} is usually lower than η_D, since the propeller usually operates at a higher propeller loading (lower advance number) in waves, so our assumption will slightly underestimate the brake power in waves. When $\eta_{Dw} < \eta_D$, the required power in waves – and thus fuel savings with wavefoils – will be higher, so by referring to lower fuel savings than in reality as "conservative", $\eta_{Dw} = \eta_D$ can be said to be a conservative simplification. Calm-water resistance and brake power curves for the case vessel without foils are shown in Fig. 4.

For both directions of each route, 1000 journeys with and without wavefoils were simulated, with wind and wave conditions obtained from ECMWF hindcast data (ECMWF, 2015). In the simulations, two identical ships, one equipped with wavefoils and the other without, started their journeys simultaneously at random times between January 1, 2000, and December 1, 2014. The brake power was set to be constant for the ship without wavefoils, whereas the ship with wavefoils reduced its power to obtain the same speed as the ship without wavefoils. For simplicity, percentage fuel savings are assumed to be equal to percentage energy savings.

The whole scatter diagram of sea states, except significant wave heights larger than 8 m, were simulated, with the wave direction ranging from head to following sea in steps of 45 degrees. The Pierson-Moskowitz wave spectrum (Pierson and Moskowitz, 1964) was used in the simulations. We did not include

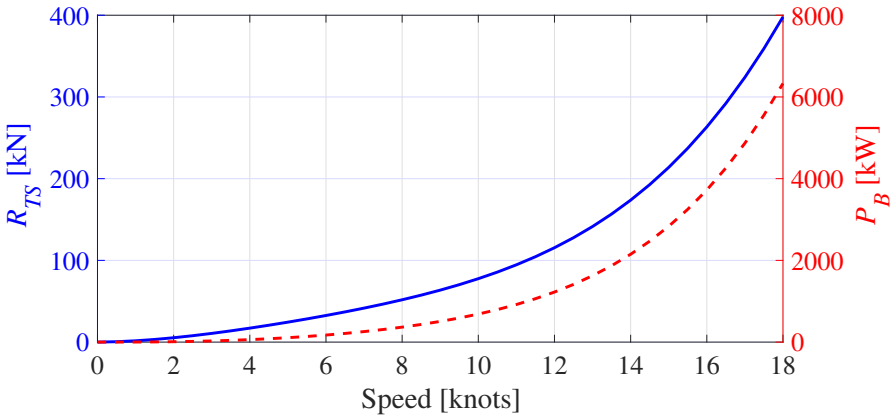

Figure 4: Calm-water resistance (R_{TS}) and brake power (P_B) for the case vessel with the wavefoils retracted. Blue solid curve is R_{TS} and red dashed curve is P_B.

journeys with higher sea states than $H_S = 8$ m in the simulations because linear theory is not valid for very large waves. In addition, the vast majority of sea states fall below this limit, see Fig. 5. If $H_S > 8$ m occurred on a simulated journey, an extra journey was made with all H_S encountered on the extra journey less than or equal to 8 m. The foils were assumed to be retracted for $H_S > 6$ m. The foils were also assumed to be retracted if having them deployed resulted in a lower speed than the ship without foils. If a section of the foil emerged from water, the forces of that section was set equal to zero until the section became submerged again.

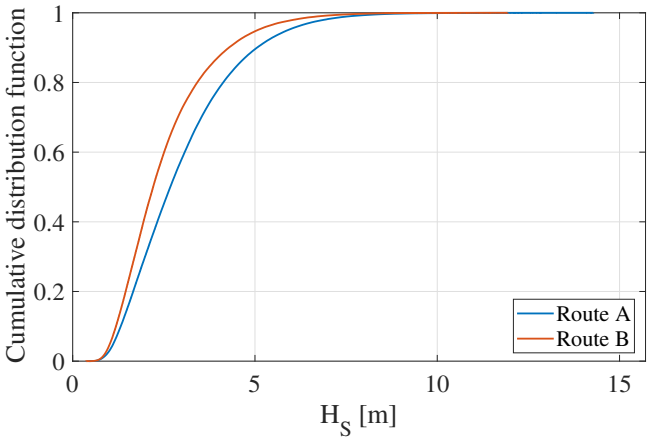

Figure 5: Cumulative distribution of significant wave heights for the two routes studied.

4.2 Added resistance due to wind

The added resistance due to wind, ΔR_{wind}, was calculated as

$$\Delta R_{wind} = -\frac{1}{2}\rho_a V_A^2 A_X C_X(\beta), \tag{3}$$

where ρ_a is the mass density of air, V_A is the apparent wind speed, A_X is the projected front area of the vessel above the waterline, and C_X is the wind coefficient in surge, which is a function of β, the apparent wind direction. In the present work we have used a $C_X(\beta)$ graph for a supply vessel from Brix (1987), which is shown in Fig. 6. The minus sign in Eg. 3 is present to produce a resistance when C_X is negative for $\beta = 0$ degrees, which is headwind, in Fig. 6.

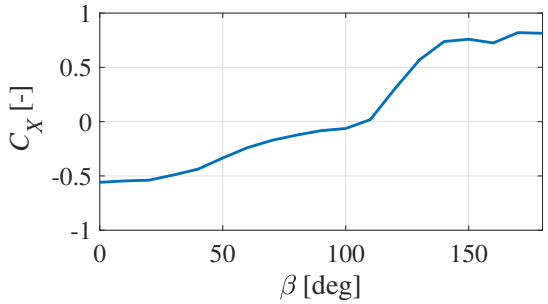

Figure 6: The wind resistance coefficient (C_X) vs. apparent wind angle β graph used in the present work. $\beta = 0$ is headwind. Data from Brix (1987).

4.3 Added resistance due to waves

As in the guidelines of the International Maritime Organization (2012), the added resistance due to irregular waves was calculated by a linear superposition of the added resistance components of regular waves:

$$\Delta R_{wave} = 2\int_{-\pi}^{\pi}\int_{0}^{\infty} \frac{R_{wave}(\omega,\alpha,V)}{\zeta_A^2} E(\omega, H_S, T_z, \alpha, \theta) d\omega d\alpha, \tag{4}$$

where R_{wave} is the added resistance due to regular waves, ω is the circular wave frequency, α is the angle between the ship course and the wave direction, E is the directional spectrum, T_z is the mean zero-up-crossing period, θ is the mean wave direction, and ζ_A is the amplitude of the regular waves. The quadratic transfer function for the added resistance in regular waves, $\frac{R_{wave}(\omega,\alpha,V)}{\zeta_A^2}$, was obtained using VERES.

In VERES, the pressure integration method of Faltinsen et al. (1980) was selected. This method is based on strip theory. The method is questionable in the small wavelength range for blunt ship forms, since strip theory neglects the effect of reflection of waves from the bow of the ship (Fathi and Hoff, 2015). Therefore it is combined with an asymptotic formula for short waves in VERES. For short waves, VERES uses the wave reflection theory of Faltinsen et al. (1980). The methods for calculating added resistance due to ship motions and

due to wave reflection are combined by following the approach of Fujii and Takahashi (1975) in such a way that for low wave lengths the added resistance is calculated purely by the wave reflection theory (Fathi and Hoff, 2015).

In Fig. 7, heave and pitch Response Amplitude Operators (RAOs) with and without foils in head seas for the speeds 0, 9 and 18 knots and are shown. We see that the motion damping effect of the foils is significant when the speed increases, which implies lower added resistance in waves. The reason why there is no motion damping effect at zero speed is because the RAOs are calculated with ShipX VERES, which is based on linear theory, i.e., zero forward speed gives zero foil lift (Bøckmann, 2015).

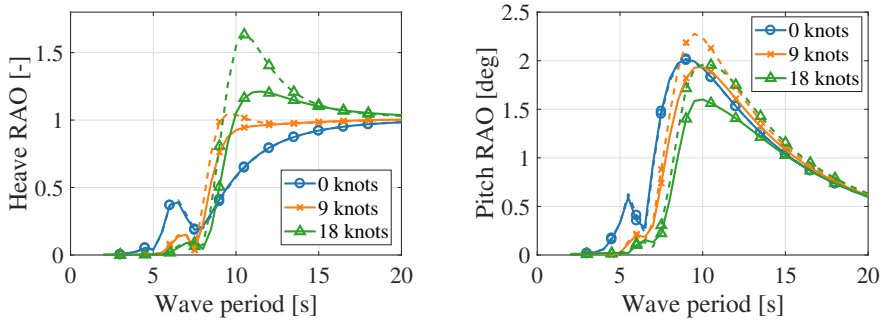

(a) Heave RAO (b) Pitch RAO

Figure 7: Heave and pitch RAOs with foils (solid lines) and without foils (dashed lines) in head seas for the speeds 0, 9 and 18 knots.

The added resistance in waves, ΔR_{wave}, is plotted against T_p with and without foils for a speed of 12 knots and H_S ranging from 2.5 to 4.5 m, head seas, in Fig. 8a. Since ΔR_{wave} is highest for $T_p = 9.1$ s, ΔR_{wave} with and without foils, head seas, is plotted against speed for $T_p = 9.1$ s and the same H_S values in Fig. 8b. We see that the foils clearly reduce the added resistance in waves, particularly for the highest speeds.

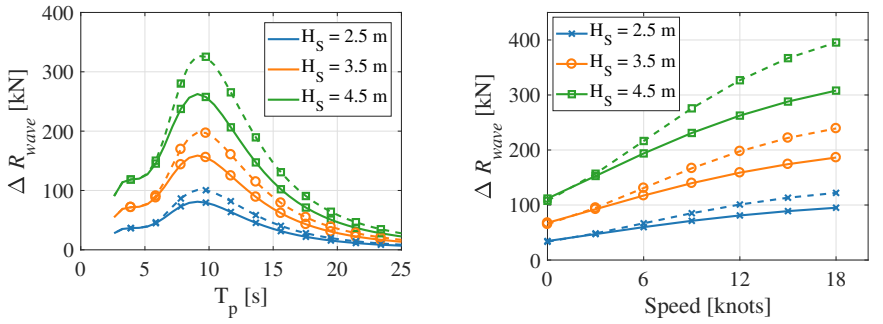

(a) Speed = 12 knots (b) $T_p = 9.1$ s.

Figure 8: Added resistance in waves with foils (solid lines) and without foils (dashed lines) in head seas.

4.4 Wavefoil thrust

The wavefoil thrust, defined here as the chordwise force on the foil, was calculated using a slightly modified Leishman-Beddoes (L-B) dynamic stall model (Leishman and Beddoes, 1989), as in previous work by the first author (Bøckmann, 2015; Bøckmann and Steen, 2016). In the model, the normal and chordwise foil force components are calculated, converted to lift and drag, corrected for finite span effects, and converted back to normal and chordwise force components.

In order to compare different calculation models for the foil thrust, we consider the following models:

1. Frequency-domain model for the ship motions with foils and quasi-static time-domain model for the foil thrust. This implies a one-way coupling from ship motions to foil forces.

2. Frequency-domain model for the ship motions with foils and dynamic stall time-domain model for the foil thrust. This implies a one-way coupling from ship motions to foil forces.

3. Time-domain model for the ship motions with foils, including a dynamic stall time-domain model for the foil forces. This implies a two-way coupling between ship motions and foil forces.

As mentioned, model 2 is the approach undertaken in the route simulations in the present work and model 3 is what is implemented in the ship simulator VeSim (see Bøckmann and Steen (2016)). Model 1 is similar to model 2, except that a quasi-static time-domain model, instead of dynamic stall model, is used for the foil thrust. In all of these three models, quasi-static lift and drag coefficients were taken from Sheldahl and Klimas (1981). Note that one change relative to Bøckmann and Steen (2016) is that Helmbold's correction for finite span effects on lift and drag of an elliptical wing (see Faltinsen (2005)) was used in the dynamic stall model in the present work rather than Prandtl's expressions for the same. However, Prandtl's lift expression for an elliptical wing was used when specifying the lift coefficient used in the VERES calculations.

Fig. 9 shows static normal force coefficent (C_N) and chordwise force coefficient (C_C) against angle of attack (α) for Reynolds number 10,000,000, based on data from Sheldahl and Klimas (1981). This is the closest Reynolds number from Sheldahl and Klimas (1981) to the operating Reynolds number for the foil in the present work. These static force coefficients are the basis for both the quasi-static foil thrust model and the dynamic stall foil thrust model. Note that the chordwise force coefficient is negative for the angle of attack range 29-49°. Semi-empirical dynamic stall models, as the one applied in the present work, are based on delaying the stall response for angles of attack somewhat higher than the static stall angle. No existing semi-empirical dynamic stall models can model the extremely complex situation where the angle of attack varies rapidly up to 180 degrees, as is the case for the ship with foils at zero forward speed.

Figs. 10-13 compare the thrust predictions from the quasi-static model and the dynamic stall model for various forward speeds, i.e., various angle of attack ranges, for $H_S = 4.5$ m, $T_p = 9.1$ s in head seas. The foil was divided into four spanwise sections, and the angle of attack and chordwise force (F_C) in Figs. 10-13 are for the innermost foil section of the port side foil. Fig. 10 shows that the dynamic stall model implemented in models 2 and 3 produces questionably

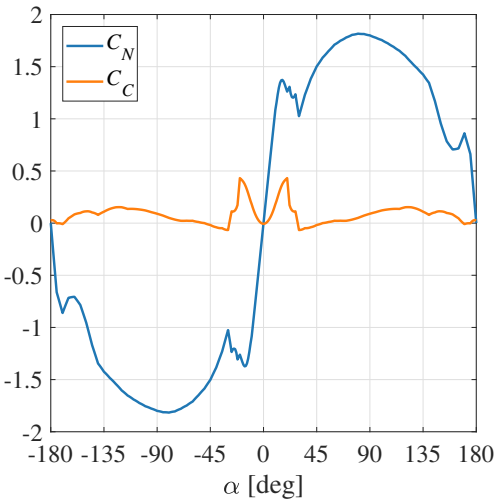

Figure 9: Static normal and chordwise force coefficient against angle of attack for Reynolds number 10,000,000, based on data from Sheldahl and Klimas (1981).

high foil thrust for zero ship speed, when comparing with the foil thrust at higher speeds, and should therefore not be trusted for very low forward speeds. We see from Fig. 13 that abrupt stall occurs for the quasi-static model when the angle of attack exceeds approximately 20 degrees, whereas the dynamic stall model maintains the chordwise force, as expected (Bøckmann, 2015). Note that for angles of attack below static stall, the quasi-static foil force model gives higher chordwise force than the dynamic stall model, which is also as expected (Bøckmann, 2015).

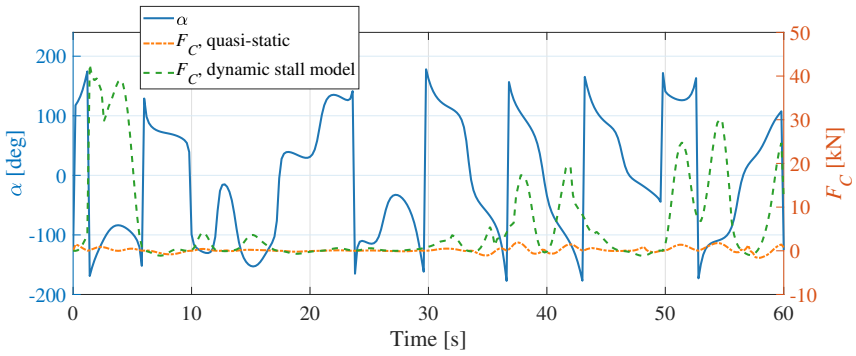

Figure 10: Angle of attack and chordwise foil force for $H_S = 4.5$ m, $T_p = 9.1$ s and a speed of 0 knots in head seas.

In Figs. 14-16, the foil thrust and the required brake power as a function of ship speed, calculated with the three calculation models described above, are shown for the same sea states in head seas as in Fig. 8b so the reader can compare the reduction of added resistance in waves with the foil thrust. Simulations were performed for speed steps of 3 knots, and the graphs are

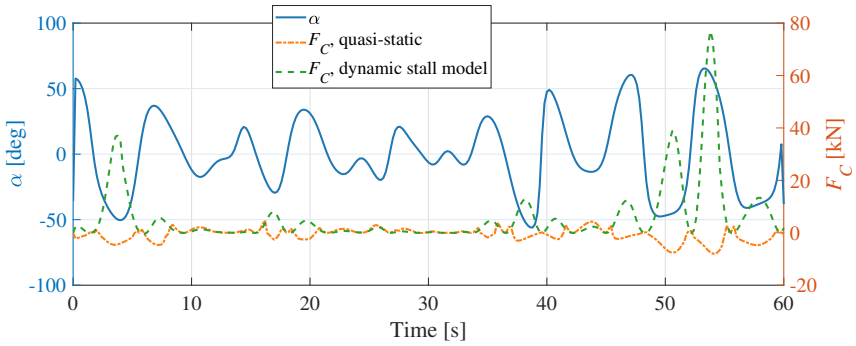

Figure 11: Angle of attack and chordwise foil force for $H_S = 4.5$ m, $T_p = 9.1$ s and a speed of 3 knots in head seas.

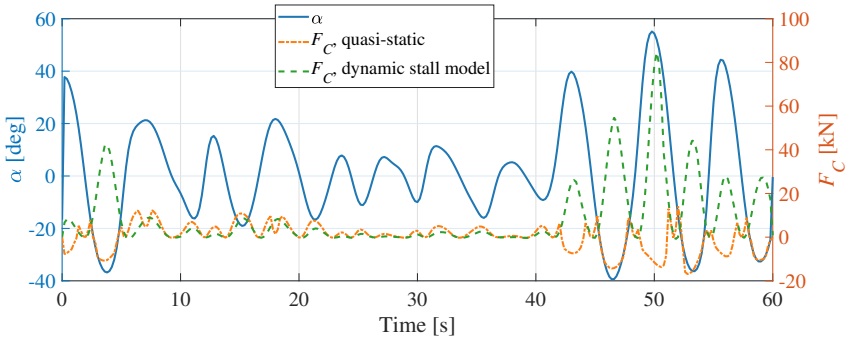

Figure 12: Angle of attack and chordwise foil force for $H_S = 4.5$ m, $T_p = 9.1$ s and a speed of 6 knots in head seas.

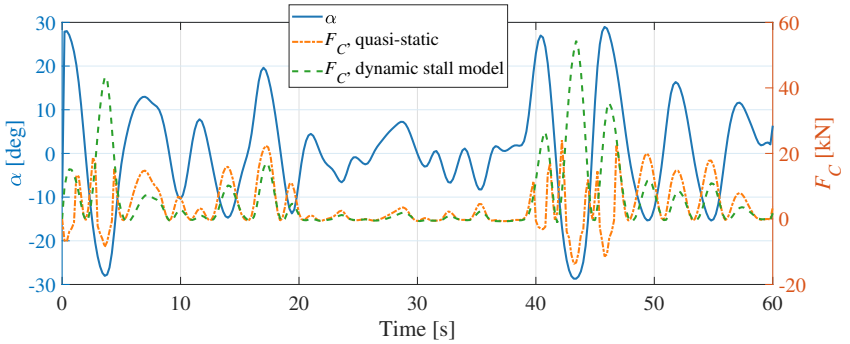

Figure 13: Angle of attack and chordwise foil force for $H_S = 4.5$ m, $T_p = 9.1$ s and a speed of 9 knots in head seas.

spline fits of the simulations results. The oscillatory shape of the T_{foils} curves in Figs. 14-16 may be better understood by examining Fig. 9 and Figs. 10-13. For extremely large angles of attack, as in Fig. 10, the dynamic stall model produces questionably high foil thrust, as already mentioned, and the quasi-static model produces near zero thrust, which is much more realistic. For more

moderate angles of attack, as in Fig. 11, the dynamic stall model still produces large thrust, but the quasi-static model now produces negative mean thrust. This makes sense when considering that the static C_C is negative in the 29-49° angle of attack range (see Fig. 9), which occurs frequently in this case. For lower angle of attacks, as in Fig. 12 and 13, we see from Fig. 9 that the static C_C is positive, and both the quasi-static and dynamic stall models will therefore produce positive thrust in these cases. As expected, the differences between the models decrease with lower wave height and higher speed, since this implies less frequent foil stalling. We also see from Figs. 14-16 that a one-way coupling from ship motions to foil force (model 2) gives lower foil thrust than a two-way coupling (model 3), which is reasonable, since foil stall will reduce the motion damping effect of the foils and thereby cause larger ship motions and foil thrust. Figs. 14-16 show that using model 2 results in higher brake power for the same speed than using model 3 and thus lower percentage reduction in brake power, compared to the case without foils. Model 2 can therefore be said to be conservative relative to model 3, which was compared with experiment results in Bøckmann (2015) and Bøckmann and Steen (2016).

To state an angle of attack range for which the dynamic stall model can be considered reasonably reliable, further experiments are needed. Based on the experiments in Bøckmann (2015) and Bøckmann and Steen (2016), however, we do consider the dynamic stall to perform quite well for angles of attack below 30 degrees.

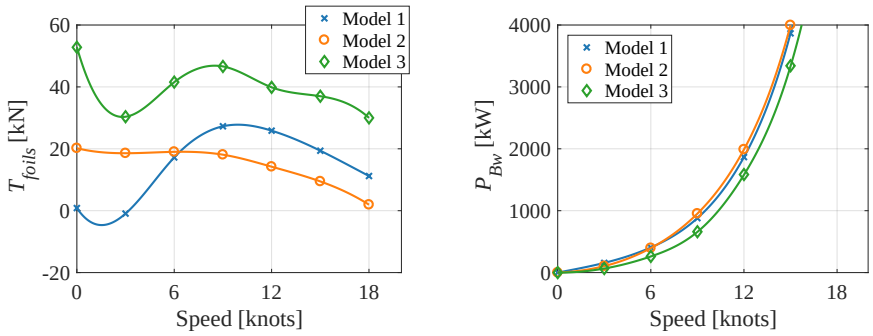

(a) Foil thrust

(b) Required brake power

Figure 14: Foil thrust (a) and required brake power (b) as a function of ship speed for $H_S = 2.5$ m, $T_p = 9.1$ s, head seas.

5 Route simulation results

Figs. 17-20 shows fuel saving histograms for the two routes, with varying values of the constant brake power without foils. The constant brake powers of 686, 1225, 2150, and 3724 kW correspond to calm-water speeds of 10, 12, 14, and 16 knots, respectively. In a severe sea state, the resulting speed will be lower, as we can see from Figs. 14b-16b. We see from Figs. 17-20 that these kind of simulations are essential to give a fair picture of the merits of the foils, as for some voyages the fuel saving is close to 100% (for low brake power), whereas for others it will be close to 0%.

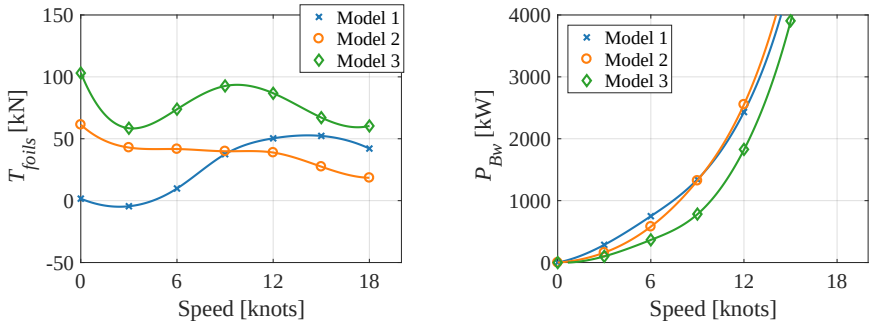

(a) Foil thrust (b) Required brake power

Figure 15: Foil thrust (a) and required brake power (b) as a function of ship speed for $H_S = 3.5$ m, $T_p = 9.1$ s, head seas.

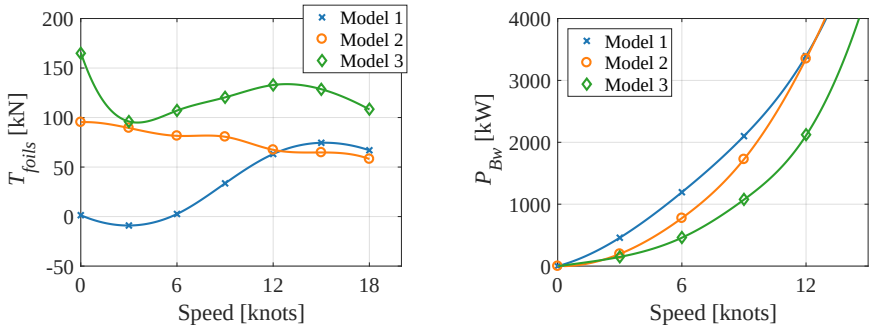

(a) Foil thrust (b) Required brake power

Figure 16: Foil thrust (a) and required brake power (b) as a function of ship speed for $H_S = 4.5$ m, $T_p = 9.1$ s, head seas.

As discussed in Sec. 4.4, the foil thrust at low speed is probably overpredicted by the dynamic stall model for low forward speeds, and the fuel saving values for low constant brake power are therefore more uncertain than for high constant brake power. Table 4 gives the mean fuel savings, based on Figs. 17-20. We see that the mean fuel savings in percent decrease with increasing power (speed) as expected.

Table 5 gives the mean fuel savings when the foil thrust is set to zero. In this case, the fuel saving is solely caused by the reduction in added resistance in waves due to reduced ship motions. Table 5 can be considered as minimum values for the fuel savings, since the uncertainty of the thrust modeling is removed by neglecting the foil thrust completely. Interestingly, when neglecting the foil thrust, the percentage fuel savings are fairly independent of speed. The corresponding fuel saving histograms when the foil thrust is set to zero are given in Appendix A.

Table 6 shows the number of simulated voyages that had to be aborted in order to complete 1000 voyages containing only sea states in the simulated H_S range (0–8 m) and T_p range (3–22 s). We see that the number of aborted voyages is small – between 0 and 4% of the total number of simulated voyages.

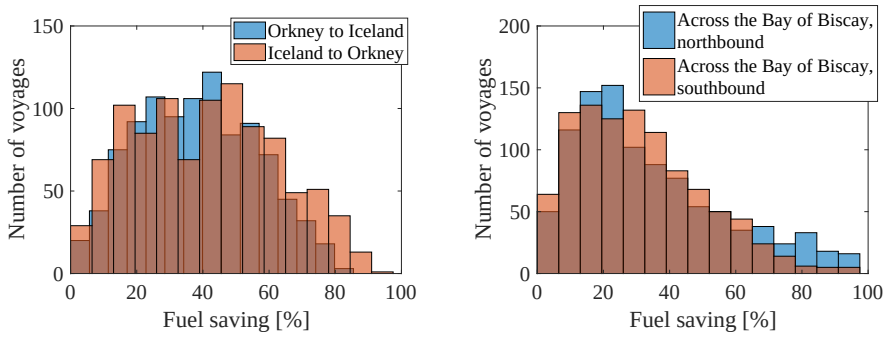

(a) Route A (b) Route B

Figure 17: Fuel saving histograms, based on 1000 simulated voyages, for a constant brake power of 686 kW without foils, corresponding to a calm-water speed of 10 knots.

	Brake power without foils [kW]			
Route	**686**	**1225**	**2150**	**3724**
Orkney - Iceland	38	29	22	16
Iceland - Orkney	41	31	21	16
Across the Bay of Biscay, northbound	34	25	17	12
Across the Bay of Biscay, southbound	31	23	17	11

Table 4: Mean fuel savings in percent.

Table 7 shows the percentage of sailing time where the foils are retracted. Also this number is quite low, having a maximum of 13% for the southbound Bay of Biscay route with a brake power without foils of 3724 kW. As expected, the retraction time increases with increasing ship speed, since higher speeds require higher waves to have forward foil thrust. Table 8 shows the percentage of sailing time where at least one part of one foil comes out water. These percentages are very low, much less than one percent.

In head seas, the foils will – at least partly – come out of water for $H_S = 4$ m and $T_p = 11$ s, at a speed of 15 knots. For $H_S = 5$ m, this occurs for a broader T_p range, and for $H_S = 6$ m the foils come out of water for most of the simulated T_p range. Given that the foils have structural integrity to handle the out-of-water events, $H_S = 6$ m may be an appropriate retraction limit, allowing the foils to be deployed and thrust-producing over the majority of sea states occuring. It is important to have in mind that it is the vertical speed of the foil as it is enters water that will cause large forces, and that a foil being partially nonsubmerged does not necessarily pose a structural challenge in itself. Structural analyses of the foil is beyond the scope of the present work, however.

In Fig. 21, the effect of number of voyages on the mean fuel saving for the Orkney–Iceland-route, for a constant brake power of 2150 kW without foils, is shown. We see that the effect of increasing the number of voyages from 100 to 1000 is minimal and that simulating 100 voyages appears to be enough for reasonably converged mean fuel savings.

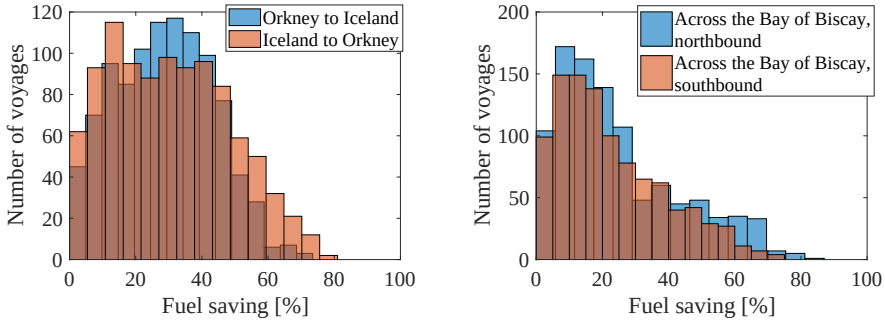

(a) Route A (b) Route B

Figure 18: Fuel saving histograms, based on 1000 simulated voyages, for a constant brake power of 1225 kW without foils, corresponding to a calm-water speed of 12 knots.

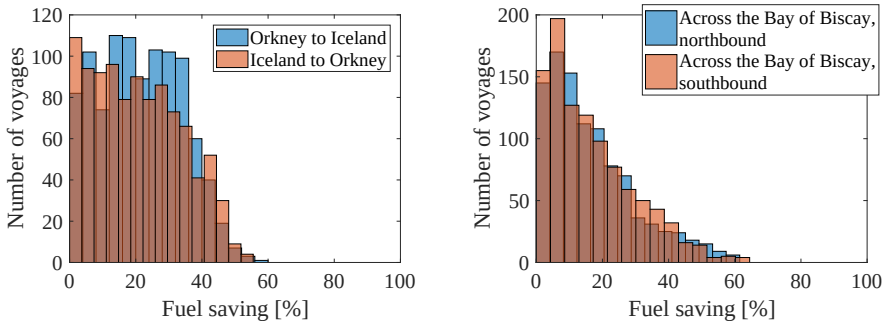

(a) Route A (b) Route B

Figure 19: Fuel saving histograms, based on 1000 simulated voyages, for a constant brake power of 2150 kW without foils, corresponding to a calm-water speed of 14 knots.

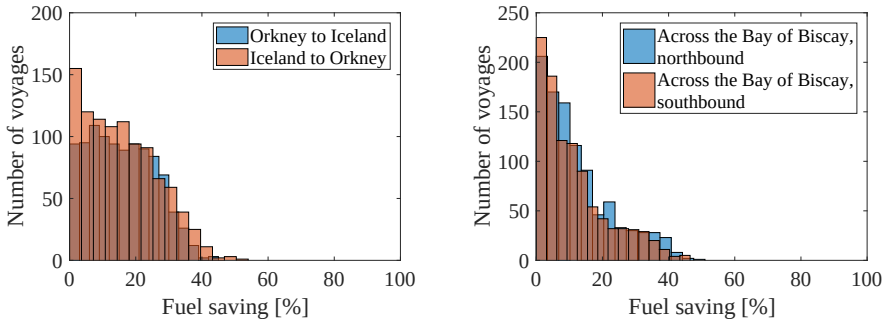

(a) Route A (b) Route B

Figure 20: Fuel saving histograms, based on 1000 simulated voyages, for a constant brake power of 3724 kW without foils, corresponding to a calm-water speed of 16 knots.

	Brake power without foils [kW]			
Route	**686**	**1225**	**2150**	**3724**
Orkney - Iceland	5	5	5	6
Iceland - Orkney	4	4	4	4
Across the Bay of Biscay, northbound	3	4	4	4
Across the Bay of Biscay, southbound	4	4	4	4

Table 5: Mean fuel savings in percent when the foil thrust is set to zero.

	Brake power without foils [kW]			
Route	**686**	**1225**	**2150**	**3724**
Orkney - Iceland	38	34	35	29
Iceland - Orkney	33	28	26	19
Across the Bay of Biscay, northbound	11	8	6	6
Across the Bay of Biscay, southbound	15	8	5	11

Table 6: Number of simulated voyages that had to be aborted in order to complete 1000 voyages containing only sea states in the simulated H_S range (0–8 m) and T_p range (3–22 s).

	Brake power without foils [kW]			
Route	**686**	**1225**	**2150**	**3724**
Orkney - Iceland	5	6	8	9
Iceland - Orkney	5	6	9	10
Across the Bay of Biscay, northbound	2	4	7	9
Across the Bay of Biscay, southbound	3	5	8	13

Table 7: Percentage of sailing time where the foils are retracted.

	Brake power without foils [kW]			
Route	**686**	**1225**	**2150**	**3724**
Orkney - Iceland	0.18	0.16	0.15	0.12
Iceland - Orkney	0.27	0.27	0.21	0.23
Across the Bay of Biscay, northbound	0.13	0.13	0.12	0.13
Across the Bay of Biscay, southbound	0.09	0.08	0.08	0.06

Table 8: Percentage of sailing time where at least one part of one foil comes out of water.

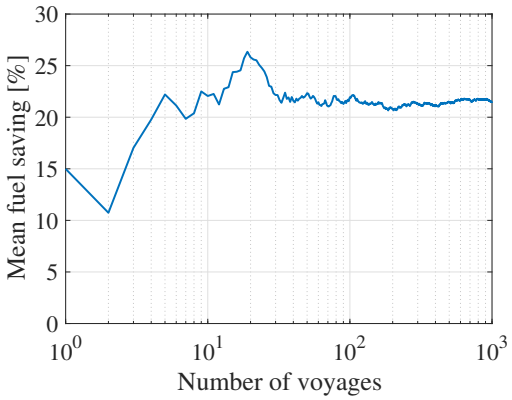

Figure 21: The effect of number of voyages on the mean fuel saving for the Orkney–Iceland-route, for a constant brake power of 2150 kW without foils, corresponding to a calm-water speed of 14 knots.

6 Conclusions

A 100 m long ship employing retractable bow-mounted foils will experience large fuel savings on wave-rich routes according to simulations. The percentage fuel savings were shown to decrease with increasing brake power but were still significant at full power. The foil thrust made up the largest part of the fuel saving effect, and modeling the foil thrust accurately is therefore of high importance for the accuracy of the calculations. A slightly modified Leishman-Beddoes dynamic stall model for the foil thrust resulted in questionably high thrust at low ship speeds. Thus, more research should be undertaken to verify or develop dynamic stall models for very large angles of attack. A one-way coupling from ship motions to foil forces was shown to give lower foil thrust than a two-way coupling, so this is a conservative approach. Finally, a number of 100 voyages appears to be enough for reasonably converged mean fuel savings.

7 Further work

The scope of the present work was to calculate average percentage fuel savings for a given ship on two selected routes. For retractable bow foils to be commercially viable, structural analyses – particularly fatigue analyses – must be performed. The structural integrity of the foils during out-of-water events, i.e. foil slamming, is essential to the feasibility of bow foils and should be studied thoroughly. Perhaps such a study will find that the retraction limit of $H_S = 6$ m needs to be lowered. One must also know the cost of constructing and installing the foils for a given ship. Obviously, the fuel savings will be less for less wave-rich routes, and analyses of such routes would also be interesting to study from an economic perspective. Further validation/improvement of the dynamic stall model, particularly for high angles of attack, would be very useful. Finally, the retraction mechanism and associated aperture drag should be investigated in more detail. Sufficient space for the retraction mechanism may be a problem, depending on the bow form and the general arrangement.

Acknowledgements

This work has been financed by the research project Low Energy and Emission Design of Ships (LEEDS), which is sponsored by DNV GL, Rolls-Royce Marine and the Norwegian Research Council (grant number 216432/O70).

References

Angvik, I. (2009). Application of an active foil propeller on an offshore vessel. Master's thesis, Norwegian University of Science and Technology.

Bøckmann, E. (2015). Wave Propulsion of Ships. PhD thesis, Norwegian University of Science and Technology.

Bøckmann, E. and Steen, S. (2013). The effect of a fixed foil on ship propulsion and motions. In Proceedings of the Third International Symposium on Marine Propulsors, pages 553–561.

Bøckmann, E. and Steen, S. (2016). Model test and simulation of a ship with wavefoils. Applied Ocean Research, 57:8–18.

Borgen, C. T. (2010). Application of an active foil propeller. Master's thesis, Norwegian University of Science and Technology.

Brix, J. (1987). Manoeuvring technical manual. Schiff und Hafen, 36(5).

ECMWF (2015). ERA Interim, Daily. Web page, retrieved 11.10.2015 from `http://apps.ecmwf.int/datasets/data/interim-full-daily`.

Faltinsen, O., Minsaas, K., Liapis, N., and Skjørdal, S. (1980). Prediction of resistance and propulsion of a ship in a seaway. In 13th Symposium on Naval Hydrodynamics, pages 505–529.

Faltinsen, O. M. (2005). Hydrodynamics of High-Speed Marine Vehicles. Cambridge University Press.

Fathi, D. (2014). ShipX Vessel Responses (VERES), Motion Control Extension. MARINTEK.

Fathi, D. and Hoff, J. R. (2015). ShipX Vessel Responses (VERES), Theory Manual. MARINTEK.

Fujii, H. and Takahashi, T. (1975). Experimental study on the resistance increase of a ship in regular oblique waves. Proc. of 14th ITTC, 4:351–360.

Hollenbach, K. U. (1998). Estimating resistance and propulsion for single-screw and twin-screw ships. Ship Technology Research, 45(2).

International Maritime Organization (2012). Interim guidelines for the calculation of the coefficient f_w for decrease in ship speed in a representative sea condition for trial use. MEPC.1/Circ.796.

Leishman, J. G. and Beddoes, T. S. (1989). A semi-empirical model for dynamic stall. Journal of the American Helicopter Society, 34(3):3–17.

Lützen, M. and Holmegaard, H. O. (2012). A model for prediction of propulsion power and emissions – tankers and bulk carriers. Paper presented at World Maritime Technology Conference, Saint-Petersburg, Russian Federation.

Naito, S. and Isshiki, H. (2005). Effect of bow wings on ship propulsion and motions. Applied Mechanics Reviews, 58(4):253–268.

Pierson, W. J. and Moskowitz, L. (1964). A proposed spectral form for fully developed wind seas based on the similarity theory of S. A. Kitaigorodskii. Journal of Geophysical Research, 69(24):5181–5190.

Salvesen, N., Tuck, E. O., and Faltinsen, O. M. (1970). Ship motions and sea loads. Transactions SNAME, 78:250–287.

Sheldahl, R. E. and Klimas, P. C. (1981). Aerodynamic characteristics of seven symmetrical airfoil sections through 180-degree angle of attack for use in aerodynamic analysis of vertical axis wind turbines. SAND80-2114, Sandia National Laboratories, Albuquerque, New Mexico.

Theodorsen, T. (1935). General theory of aerodynamic instability and the mechanism of flutter. NACA Tech. Rep. 496.

Veritec (1985). Analysis of a foil propeller as an auxiliary propulsion system. Veritec report 85-3326.

Veritec (1986). Analysis of a foil propeller as an auxiliary propulsion system. Veritec report 86-3413.

A Fuel saving histograms with no wavefoil thrust

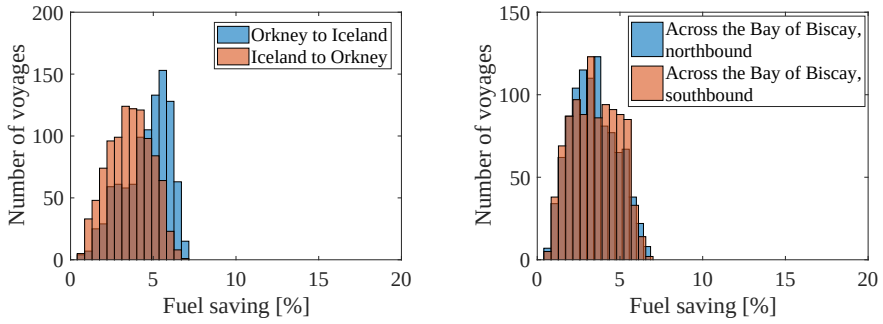

(a) Route A (b) Route B

Figure 22: Fuel saving histograms with zero foil thrust, based on 1000 simulated voyages, for a constant brake power of 686 kW without foils, corresponding to a calm-water speed of 10 knots.

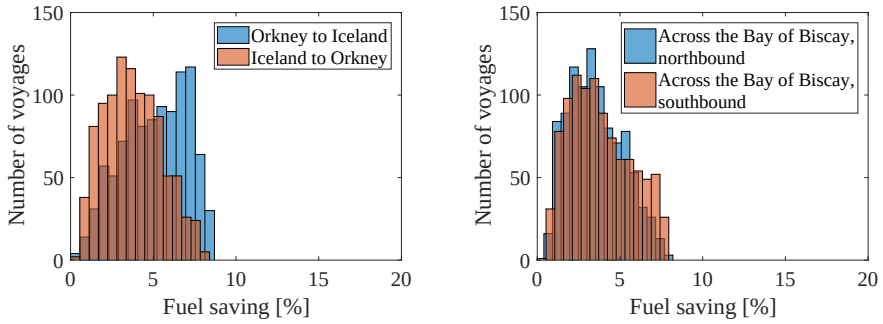

(a) Route A (b) Route B

Figure 23: Fuel saving histograms with zero foil thrust, based on 1000 simulated voyages, for a constant brake power of 1225 kW without foils, corresponding to a calm-water speed of 12 knots.

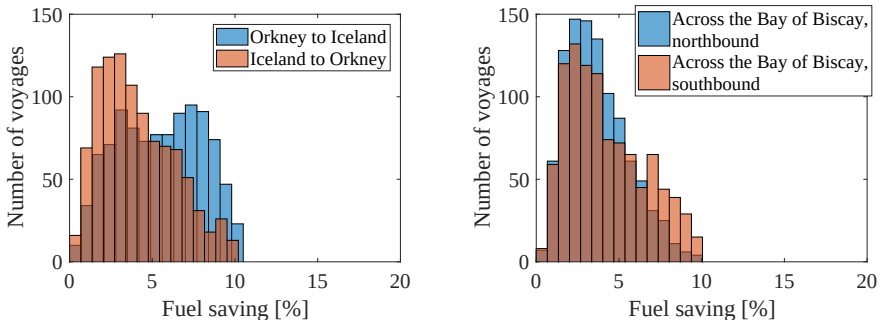

(a) Route A (b) Route B

Figure 24: Fuel saving histograms with zero foil thrust, based on 1000 simulated voyages, for a constant brake power of 2150 kW without foils, corresponding to a calm-water speed of 14 knots.

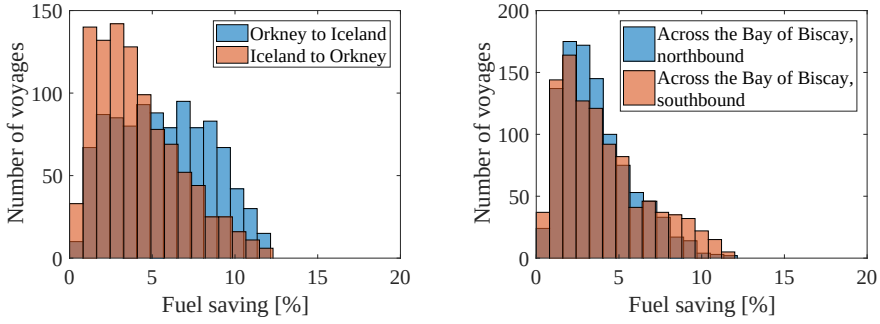

(a) Route A (b) Route B

Figure 25: Fuel saving histograms with zero foil thrust, based on 1000 simulated voyages, for a constant brake power of 3724 kW without foils, corresponding to a calm-water speed of 16 knots.